SUPPORTING INFORMATION

Sulfide Protects [FeFe] Hydrogenases From O_2

Patricia Rodríguez-Maciá[†], Edward J. Reijerse[†], Maurice van Gastel[I], Serena DeBeer[†], Wolfgang Lubitz[†], Olaf Rüdiger*[†], James A. Birrell*[†]

[†]Max Planck Institute for Chemical Energy Conversion, Stiftstraße 34-36, D-45470 Mülheim an der Ruhr, Germany
[I]Max-Planck-Institut für Kohlenforschung, Kaiser-Wilhelm-Platz 1, D-45470 Mülheim an der Ruhr, Germany

Materials and methods

Sample preparation

*Cr*HydA1, *Cp*HydA1 and *Dd*HydAB were produced recombinantly in *Escherichia coli* and artificially maturated as described previously.[1,2] $(Et_4N)_2[Fe_2(adt)(CO)_4(CN)_2]$ ([2Fe]^{adt}) was synthesized as previously reported.[3]

FTIR spectroscopy and spectro-electrochemistry

FTIR spectroscopy was performed on 10 µL samples of 0.2 mM *Dd*HydAB (in 50 mM MES, 50 mM HEPES, 300 mM KCl, pH 8, prepared under an atmosphere of N_2) fixed between CaF_2 windows (20 mm x 4 mm, Korth Kristalle, Altenholz) separated with a 50 µm Teflon spacer coated with vacuum grease and closed in homebuilt IR cells with rubber rings. The temperature of the cell was maintained at 25 °C using a water circulator system (Huber, Offenburg). Spectra were measured on a Bruker IFS 66v/S FTIR spectrometer equipped with a nitrogen cooled Bruker mercury cadmium telluride (MCT) detector. Spectra were collected in the double-sided, forward-backward mode with a resolution of 2 cm^{-1}, an aperture setting of 1.5 mm and a scan velocity of 20 Hz. Spectra are the average of 1000 scans. Data were processed using home-written routines in the MATLAB™ environment. Spectro-electrochemistry experiments were performed as described previously[4] using a homebuilt spectro-electrochemical IR cell, constructed according to an original design by Moss and co-workers.[5] Samples (45 µL) of 1-2 mM *Dd*HydAB containing 0.5 mM of the redox mediators anthraquinone-1,5-disulfonic acid (E_{m7} = –234 mV), anthraquinone-2-sulfonate (E_{m7} = –277 mV), benzyl viologen (E_m = –358 mV), methyl viologen (E_m = –449 mV) and 1,1',2,2'-Tetramethyl-[4,4'-bipyridine]-1,1'-diium iodide (E_m= -540 mV) were loaded between CaF_2 windows on a gold mesh (≈ 50 µm thick), which was used as a working electrode. A platinum counter electrode and a Ag/AgCl (sat. KCl) reference electrode completed the three-electrode system. The reference electrode was calibrated before and after each measurement using (hydroxymethyl)ferrocene (Aldrich, +420 mV vs SHE) as a reference, to ensure the potential stability during the course of the experiment. The potential was controlled by an Autolab PGSTAT101 potentiostat using Nova software with an equilibration time of 15 min at each potential. All potentials referred to in the text are quoted versus the standard hydrogen electrode (SHE).

Electrochemistry

For covalent attachment of *Dd*HydAB pyrolytic graphite electrodes (0.031 cm^2, homemade using pyrolytic graphite from Momentive Materials) were modified with 4-nitrobenzenediazonium salt (Alfa Aesar) following the protocol described previously.[6] Once the electrode was modified, it was taken inside an N_2 glovebox (MBraun) and 10 cycles of voltammetry from +0.241 V to -0.659 V (*vs* SHE) were performed to remove the oxygen adsorbed on the electrode surface. Next, *Dd*HydAB was immobilized by covering the electrode with 6 µL of 10 µM protein diluted in 10 mM MES pH 5.8. The enzyme was left to adsorb for 20 min. Subsequently, 4.5 µL of 128 mM N-hydroxysuccinimide (NHS) and 5.5 µL of 210 mM N-(3-dimethylaminopropyl)-N`-ethylcarbodiimide (EDC), both in 10 mM MES pH 5.8, were added to the electrode and left to react for 90 min. For the non-covalent adsorption of *Cr*HydA1 and *Cp*HydA1, pyrolytic graphite electrodes were first polished with alumina MasterPrep Polishing Suspension 0.05 mm (Buehler, Esslingen, Germany) and sonicated for 5 min in Milli-Q water outside the glovebox. Afterwards, they were transferred to the glovebox and oxygen adsorbed to the surface was removed by consecutive voltammetry cycles. For the protein adsorption, in both cases 4 µL of 6 µM enzyme solution in 10 mM MES pH 5.8 were dropped on the electrode surface and allowed to adsorb for 5 min, after which the non-bound enzyme was removed by rinsing with water before transferring the electrode to the electrochemical cell. The potential was controlled by a VersaSTAT 4-400 potentiostat, and a temperature in the electrochemical cell of 15 ^oC was controlled by a water-jacket system and a water circulator (Lauda). Electrochemical measurements were carried out in a standard three-electrode electrochemical cell with a saturated calomel reference electrode (SCE) separated from the main compartment in a sidearm containing 0.1 M KCl, connected to the main cell compartment by a Luggin capillary. Platinum wire was used as a counter electrode. The reference electrode was calibrated using (hydroxymethyl)ferrocene (Aldrich) (E^0 = +436 mV) as a reference.[7] A set of mass flow-controllers (Brooks Instruments) was used to control the gas composition flushed through the electrochemical cell. Gases were flushed through an O_2 filter (Air Liquide) before going through the cell to avoid any O_2 contamination. For the O_2 tolerance experiments volumes of O_2 saturated buffer solutions were injected to have a final concentration of 273 µM in the electrochemical cell. All the experiments were performed in a buffer at pH 7 containing a mixture of 15 mM MES, HEPES, TAPS, CHES and sodium acetate as well as 0.1 M NaCl. All potentials are quoted versus the standard hydrogen electrode (SHE).

Resonance Raman spectroscopy

Resonance Raman spectroscopy was performed on a 1 mM sample of *Dd*HydAB in the H_{ox}^{air} state in 5 mm o.d. quartz tubes. Raman spectra were recorded on a TriVista 555 triple monochromator equipped with a liquid-nitrogen-cooled Roper Scientific 400BR Excelon CCD camera, using a Cobolt diode laser at 457 nm and 50 mW power. The sample temperature was maintained at 100 K using an Oxford Cryostream 800 system. The Raman light was collected in a 180° backscattering geometry using a protected silver off-axis parabolic mirror and focused onto the entrance slit of a spectrograph with a 100 mm diameter f/4 lens. Data were processed using home-written routines in MATLAB™.

Supplementary Discussion

The mechanism of H_{ox}^{air} formation/reactivation

As shown in Figure 4 and briefly described in the main text, we speculate that the H_{ox}^{air} state forms when *Dd*HydAB is strongly oxidized in the presence of sulfide by the following mechanism. When the enzyme is in the H_{ox} state, it is capable of binding H_2S. It is highly unlikely that a significant amount of S^{2-} exists in solution and, while HS^- should be available, anions are highly unlikely to enter the hydrophobic gas channel leading to the open coordination site on the H-cluster. When H_2S binds, the additional proton may equilibrate between the HS^- ligand and the NH group of the bridging dithiolate ligand. This would resemble somewhat the situation when H_2 binds to the H-cluster. This state is most likely to be quickly stabilized by a reducing equivalent moving from the [2Fe] sub-cluster to the [4Fe-4S] sub-cluster coupled to deprotonation of the bridging NH_2^+ group, where the proton can then enter the proton channel. This type of proton coupled electronic rearrangement was already demonstrated to occur in the one-electron reduced active state of the enzyme ($H_{red}/H_{red}H^+$)[8] and is proposed to occur in the two electron reduced state ($H_{hyd}/H_{hyd}H^+$) also.[9] This forms the H_{trans} state characterized by a reduced $[4Fe\text{-}4S]_H$ and an oxidized $[2Fe]_H$ in a homovalent Fe(II)Fe(II) configuration with an additional ligand at the open coordination site, which we propose to be HS^-. Oxidation of the [4Fe-4S] sub-cluster then gives the H_{ox}^{air} state. In the reverse direction (i.e. the reactivation of H_{ox}^{air}) reduction of H_{ox}^{air} to H_{trans} proceeds by reduction of $[4Fe\text{-}4S]_H$. H_{trans} should convert spontaneously to H_{ox} by release of H_2S, however, the H_{trans} state is likely to be quite stable and so this process is slow. Further reduction occurs at the proximal F-cluster, leading to anti-cooperativity between the proximal F-cluster and the $[4Fe\text{-}4S]_H$ sub-cluster,[10] and hence forcing proton-coupled electronic rearrangement of the H-cluster with concomitant release of the HS^- ligand in the form of H_2S. This would suggest that the ultimate product of H_{ox}^{air} reactivation is an H_{ox} state in which the proximal F-cluster is reduced, which should have been observed in the previously published EPR redox titrations of the H_{ox}^{air} state. In fact, [4Fe-4S] cluster EPR signals were observed to increase in intensity concomitantly with the formation of the H_{ox} state.[11,12] We further note that during the oxidative FTIR spectro-electrochemical titration non-Nernstian behavior is observed for the $H_{red}H^+/H_{ox}$ transition (kink in the titration curve around -400 mV, Figure S9, red curve) due to small shifts in the FTIR peak of the H_{ox} state, which occur upon oxidation of the proximal F-cluster, as noted previously.[10] Such behavior was not observed in the reductive titration (Figure S9, blue curve), suggesting that the H_{ox} state formed after the H_{trans}/H_{ox} transition has a reduced proximal F-cluster.

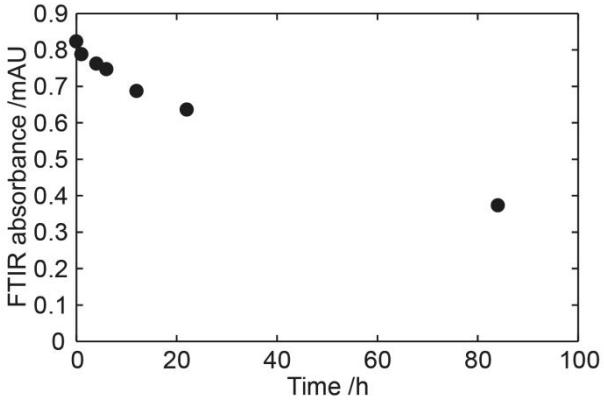

Figure S1 - Stability of *Dd*HydAB under air. A sample (0.2 mM) of *Dd*HydAB in the H_{ox}^{air} state was incubated on the bench at room temperature and at time points 10 μL samples were transferred to an FTIR cell and FTIR spectra were measured. The absorbance at 1847 cm^{-1} is plotted against time.

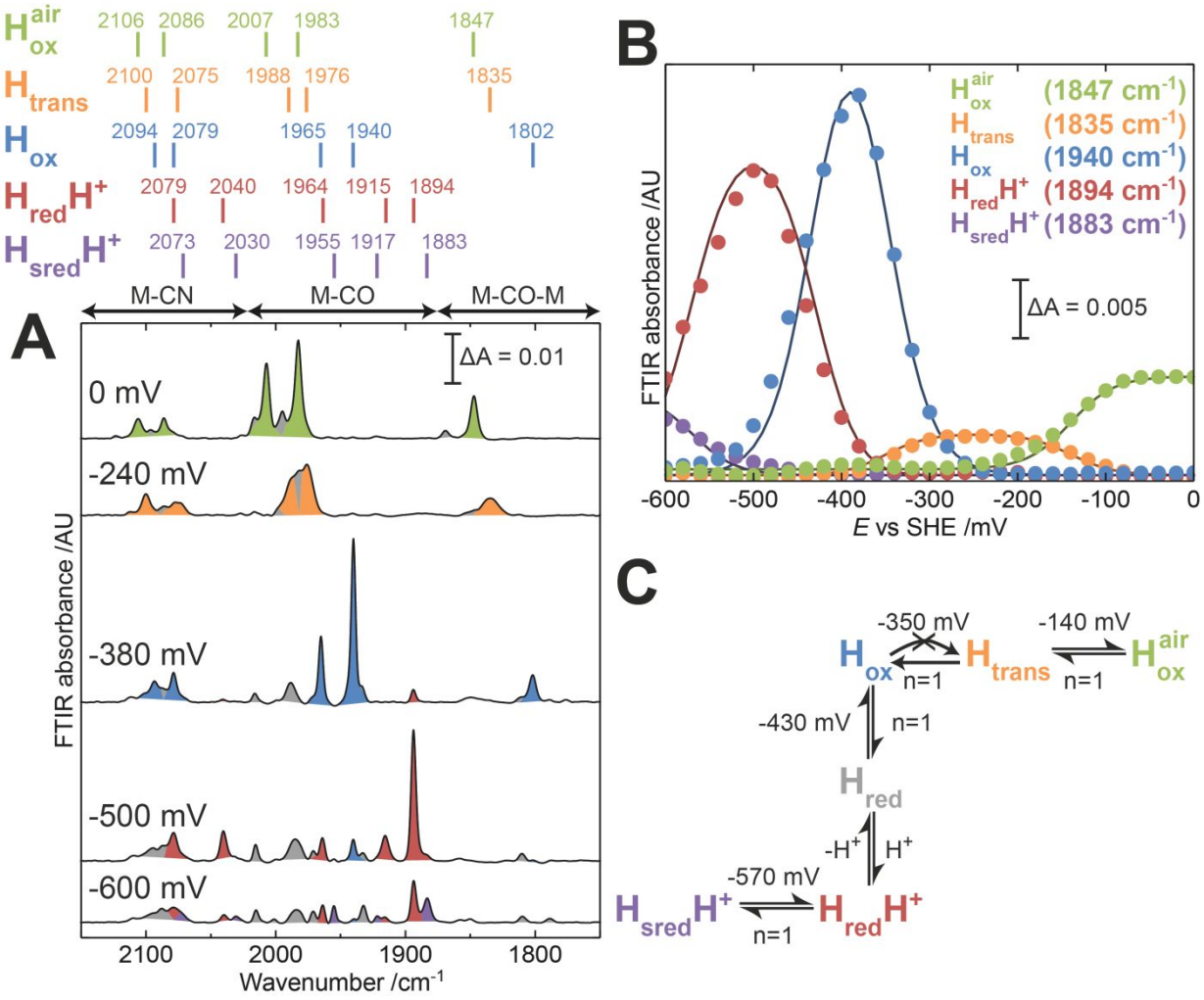

Figure S2 - FTIR spectro-electrochemistry of *Dd*HydAB in the H_{ox}^{air} state. FTIR spectra at selected applied potentials are shown (A) to highlight the main states observed during the redox titration: H_{ox}^{air} (green), H_{trans} (orange), H_{ox} (blue), $H_{red}H^+$ (red), $H_{sred}H^+$ (purple). The signal intensity of the main peaks in each state are plotted against the applied potential (B) and fitted with the Nernst equation (n = 1) to derive the midpoint potentials of each of the transitions. A scheme illustrating the various redox transitions with the associated midpoint potentials is shown (C).

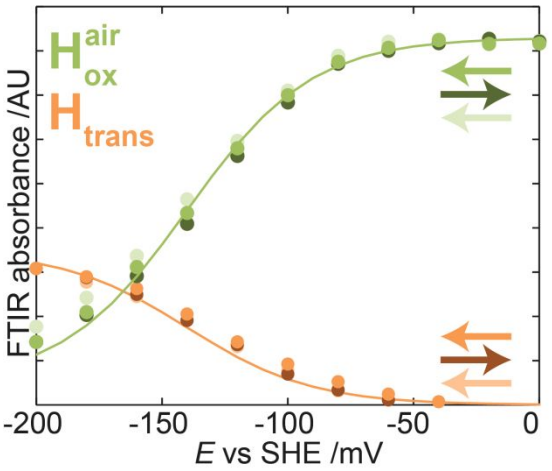

Figure S3 - Reversible transition from H_{ox}^{air} to H_{trans} states during FTIR spectro-electrochemistry of *Dd*HydAB. The signal intensity of the main peaks in the H_{ox}^{air} (green circles, 1847 cm^{-1}) and H_{trans} (orange circles, 1835 cm^{-1}) states are plotted against the applied potential and fitted with the Nernst equation (n = 1). Arrows on the right indicate the direction of the titration.

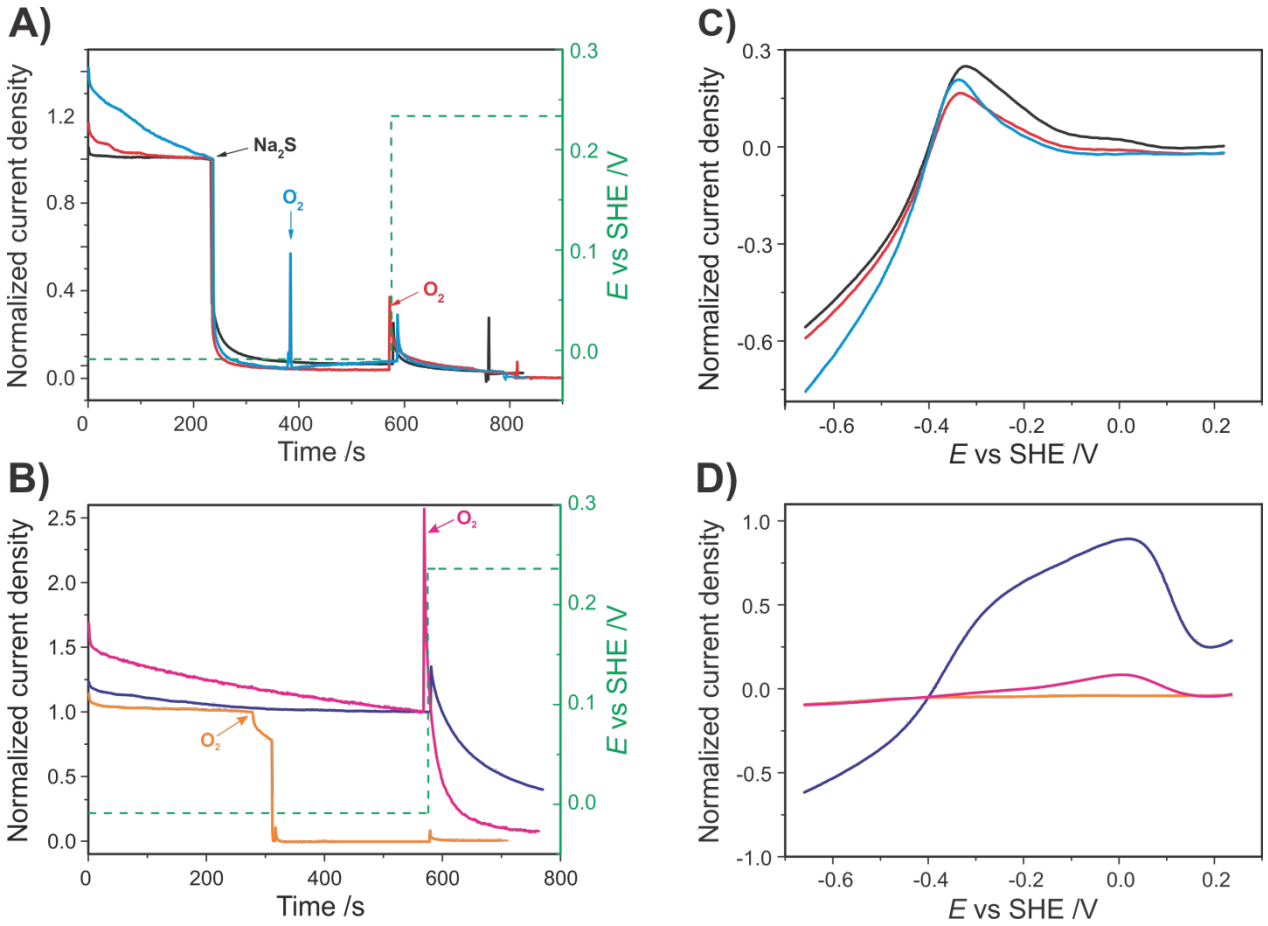

Figure S4 - Oxygen protection during oxidative sulfide inhibition of *Dd*HydAB on an electrode. **A, B:** Chronoamperometry experiments of *Dd*HydAB showing (**A**) addition of Na_2S at -9 mV (black trace), addition of Na_2S and O_2 at -9 mV (blue trace) and addition of Na_2S at -9 mV and O_2 at +241 mV (red trace). The arrows indicate the exact time points of O_2 addition to the cell. **B** shows the same experiments as in **A** but excluding Na_2S: no O_2 (blue trace), O_2 at +241 mV (pink trace) and O_2 at -9 mV (orange trace). The dotted green line in **A** and **B** represents the potential steps followed (y-axis). **C, D:** Linear scan voltammetry showing reactivation of the enzyme after (**C**) the experiments performed in **A** and (**D**) the experiments performed in **B**. The buffer was exchanged to remove the excess Na_2S and/or oxygen before performing the reactivation in **C** and **D**. It can be seen in **C** that in each case the current is completely recovered indicating that the species formed upon inactivation with Na_2S is protected from O_2. In all cases, the switch potential is essentially the same as that shown in the experiments in Figure 3 of the main text. In **D** it can be seen that when O_2 is added at high potential (+250 mV) most of the current is recovered at the typical switch potential of the high potential inactivated state but when O_2 is added at low potential (-9 mV) no current is recovered indicating that the enzyme has been irreversibly inactivated by O_2. The data in **A** and **C** are normalized to the current density at the end of the first 200 s before addition of Na_2S and the data in **B** and **D** are normalized to the current density after 550 s for the blue and pink traces (before switching to high potential) and after 250 s for the orange trace (before addition of O_2).

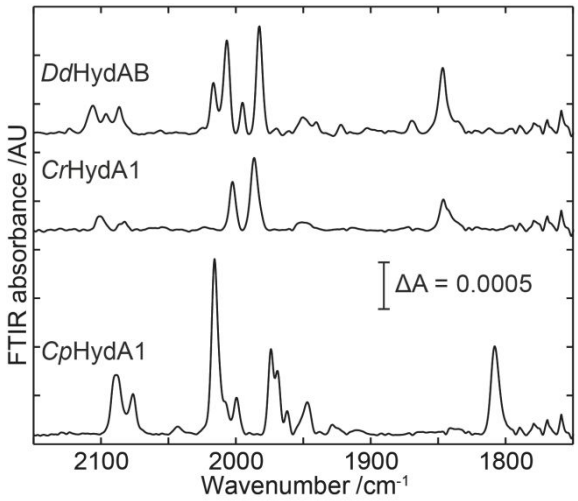

Figure S5 - Formation of H_{ox}^{air} states in *Dd*HydAB, *Cr*HydA1 and *Cp*HydA1. Samples (0.1 mM) of *Dd*HydAB (top), *Cr*HydA1 (middle) and *Cp*HydA1 (bottom) were treated with 1 mM hexaammineruthenium (III) chloride, 10 mM Na_2S and then exposed to air. The samples were then transferred to FTIR cells and FTIR spectra were measured.

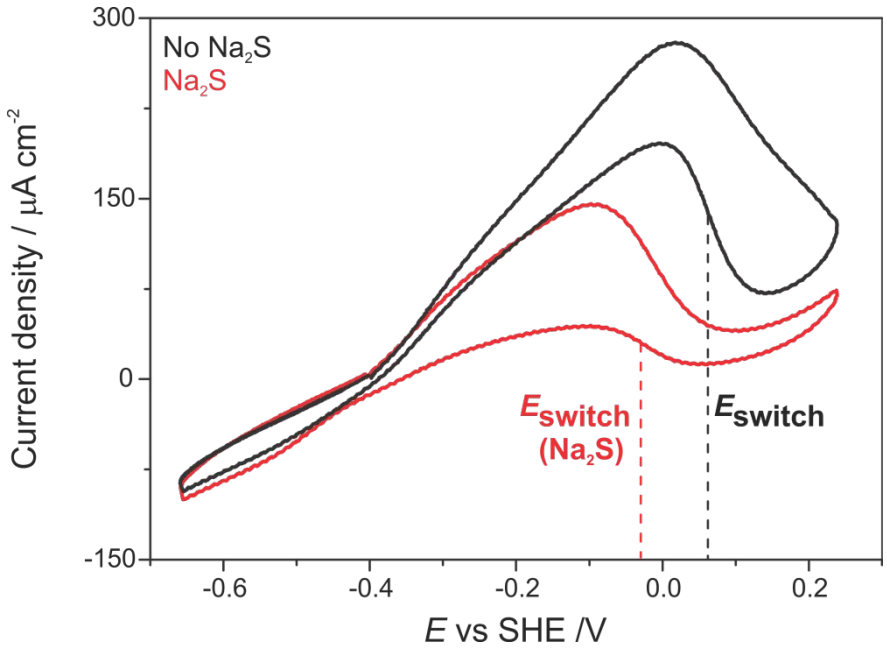

Figure S6 - Electrochemical inactivation and reactivation of *Cr*HydA1 with Na_2S. Cyclic voltammograms of *Cr*HydA1 adsorbed on a pyrolytic graphite electrode surface in the presence (red) and absence (black) of 1 mM Na_2S. Conditions: 100% H_2 (1 L min^{-1}), pH 7, 25 ºC, 2000 rpm rotation rate, 10 mV s^{-1} scan rate.

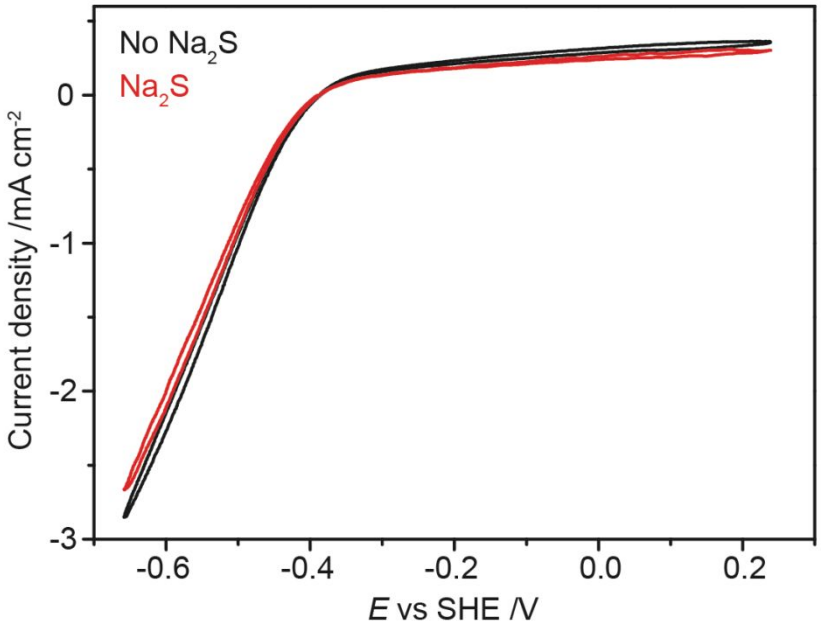

Figure S7 - Electrochemistry of *Cp*HydA1 with and without Na_2S. Cyclic voltammograms of *Cp*HydA1 adsorbed on a pyrolytic graphite electrode surface in the presence (red) and absence (black) of 1 mM Na_2S. Conditions: 100% H_2 (1 L min^{-1}), pH 7, 25 ºC, 2000 rpm rotation rate, 10 mV s^{-1} scan rate.

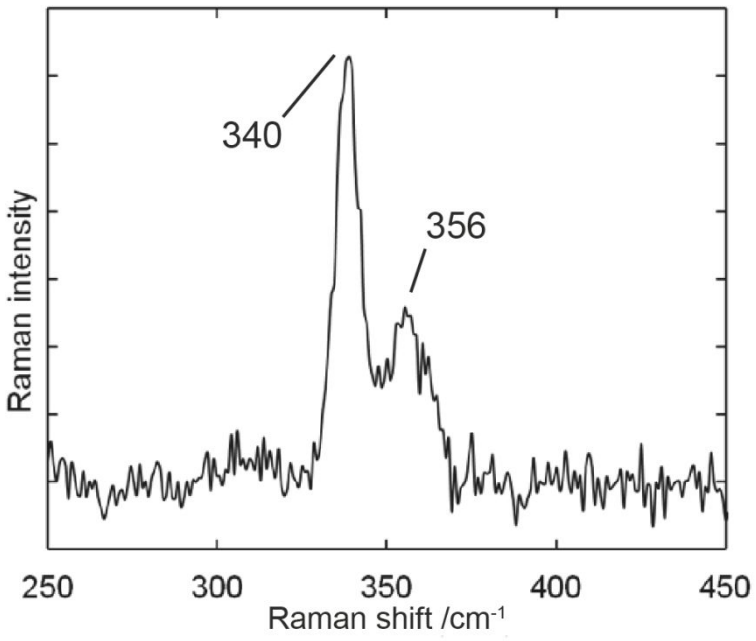

Figure S8 – Resonance Raman spectrum of H_{ox}^{air}. The resonance Raman spectrum is presented for recombinantly produced *Dd*HydAB after oxidative sulfide treatment. The spectrum was recorded with laser excitation at 457 nm at a sample temperature of 100 K. The spectrum is very similar to that published for the native H_{ox}^{air} state.[13]

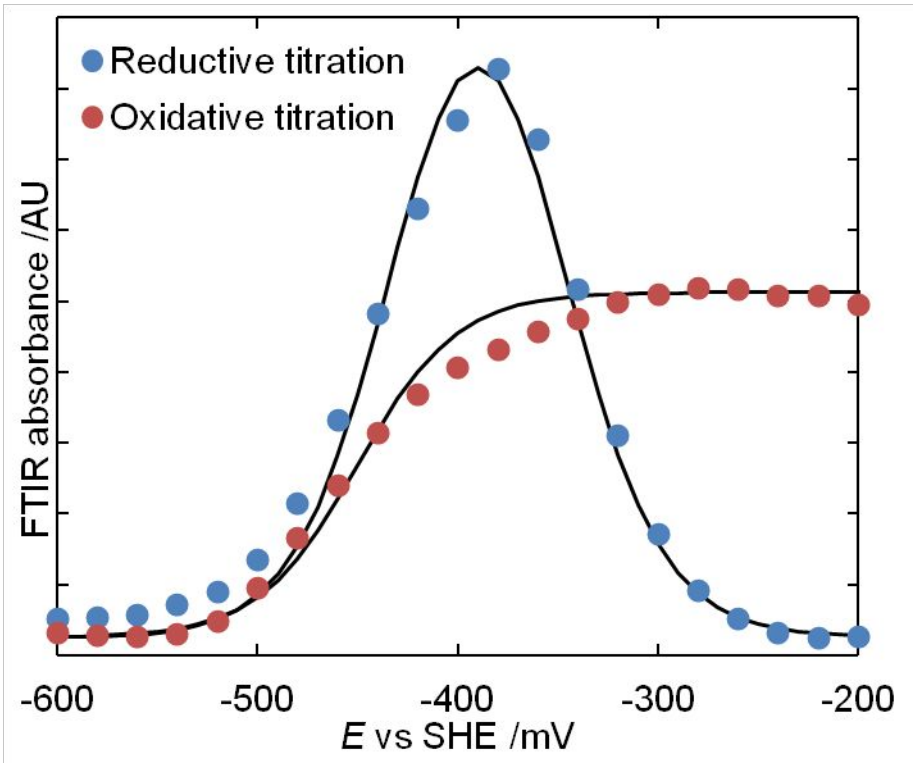

Figure S9 – Comparison of oxidative and reductive FTIR spectro-electrochemical titrations of the 1940 cm^{-1} peak from the H_{ox} state. The reductive titration (blue circles) follows the formation of H_{ox} from H_{trans} between -200 mV and -400 mV and its disappearance as $H_{red}H^+$ is formed. The oxidative titration (red circles) follows the reappearance of H_{ox} as $H_{red}H^+$ is oxidized. The black curves represent fitting to the Nernst equation with n = 1. Deviation from Nernstian behavior can be observed during the reductive titration between -400 mV and -300 mV.

Supplementary References

(1) Birrell, J. A.; Wrede, K.; Pawlak, K.; Rodríguez-Maciá, P.; Rüdiger, O.; Reijerse, E. J.; Lubitz, W. *Isr. J. Chem.* **2016**, *56*, 852.
(2) Esselborn, J.; Lambertz, C.; Adamska-Venkatesh, A.; Simmons, T.; Berggren, G.; Noth, J.; Siebel, J.; Hemschemeier, A.; Artero, V.; Reijerse, E.; Fontecave, M.; Lubitz, W.; Happe, T. *Nat. Chem. Biol.* **2013**, *9*, 607.
(3) Li, H.; Rauchfuss, T. B. *J. Am. Chem. Soc.* **2002**, *124*, 726.
(4) Rodríguez-Maciá, P.; Reijerse, E.; Lubitz, W.; Birrell, J. A.; Rüdiger, O. *J. Phys. Chem. Lett.* **2017**, *8*, 3834.
(5) Moss, D.; Nabedryk, E.; Breton, J.; Mantele, W. *Eur. J. Biochem.* **1990**, *187*, 565.
(6) Rodríguez-Maciá, P.; Birrell, J. A.; Lubitz, W.; Rüdiger, O. *ChemPlusChem* **2017**, *82*, 540.
(7) Rodríguez-Maciá, P.; Dutta, A.; Lubitz, W.; Shaw, W. J.; Rüdiger, O. *Angew. Chem. Int. Ed. Engl.* **2015**, *54*, 12303.
(8) Sommer, C.; Adamska-Venkatesh, A.; Pawlak, K.; Birrell, J. A.; Rüdiger, O.; Reijerse, E. J.; Lubitz, W. *J. Am. Chem. Soc.* **2017**, *139*, 1440.
(9) Pelmenschikov, V.; Birrell, J. A.; Pham, C. C.; Mishra, N.; Wang, H.; Sommer, C.; Reijerse, E.; Richers, C. P.; Tamasaku, K.; Yoda, Y.; Rauchfuss, T. B.; Lubitz, W.; Cramer, S. P. *J. Am. Chem. Soc.* **2017**, *139*, 16894.
(10) Rodríguez-Maciá, P.; Pawlak, K.; Rüdiger, O.; Reijerse, E. J.; Lubitz, W.; Birrell, J. A. *J. Am. Chem. Soc.* **2017**, *139*, 15122.
(11) Patil, D. S.; Moura, J. J.; He, S. H.; Teixeira, M.; Prickril, B. C.; DerVartanian, D. V.; Peck, H. D., Jr.; LeGall, J.; Huynh, B. H. *J. Biol. Chem.* **1988**, *263*, 18732.
(12) Pierik, A. J.; Hagen, W. R.; Redeker, J. S.; Wolbert, R. B.; Boersma, M.; Verhagen, M. F.; Grande, H. J.; Veeger, C.; Mutsaers, P. H.; Sands, R. H.; . *Eur. J. Biochem.* **1992**, *209*, 63.
(13) Fu, W.; Drozdzewski, P. M.; Morgan, T. V.; Mortenson, L. E.; Juszczak, A.; Adams, M. W. W.; He, S. H.; Peck, H. D.; DerVartanian, D. V. *Biochemistry* **1993**, *32*, 4813.